DTU Library

Outdoor Electroluminescence Acquisition Using a Movable Testbed

Benatto, Gisele Alves dos Reis; Mantel, Claire; Riedel, Nicholas; Santamaria Lancia, Adrian Alejo; Thorsteinsson, Sune; Poulsen, Peter Behrensdorff; Forchhammer, Søren; Thorseth, Anders; Dam-Hansen, Carsten; Kenn H. B., Frederiksen

Outdoor Electroluminescence Acquisition Using a Movable Testbed

Gisele A. dos Reis Benatto[1], Claire Mantel[1], Nicholas Riedel[1], Adrian A. Santamaria Lancia[1], Sune Thorsteinsson[1], Peter B. Poulsen[1], Søren Forchhammer[1], Anders Thorseth[1], Carsten Dam-Hansen[1], Kenn H. B. Frederiksen[2], Jan Vedde[3], Michael Larsen[4], Henrik Voss[4], Harsh Parikh[5], Sergiu Spataru[5] and Dezso Sera[5]

[1]Department of Photonics Engineering, Technical University of Denmark, Frederiksborgvej 399, 4000, Roskilde, Denmark,
[2]Kenergy, Grønningen 43, 8700, Horsens, Denmark
[3]SiCon Silicon & PV consulting, J N Vinthersvej 5, 3460, Birkerød, Denmark
[4]Sky-Watch A/S, Østre Alle 6 Støvring, 9530, Nordjylland, Denmark
[5]Aalborg University, Pontoppidanstraede 101, 9220, Aalborg, Denmark

Abstract — **The experimentation with a movable outdoor electroluminescence (EL) testbed is performed in this work. For EL inspections of PV power plants, the fastest scenario will include the use of unmanned aerial vehicle (UAV) performing image acquisition in continuous motion. With this motivation, we investigate the EL image quality of an acquisition in motion and the extent of image processing required to correct scene displacement. The results show processed EL images with a high level of information even when acquired at 1 m/s camera speed and at frame rate of 120 fps.**

Index Terms — **Electroluminescence, PV inspections, PV reliability.**

I. INTRODUCTION

The addition of 74 GW of photovoltaics capacity occurred around the world only in 2016, overcoming the growth of any other energy producing fuel for the first time [1]. Such elevate number of power implies that a very high number of modules have been installed and are subjected to many failure sources provoked by material aging, unnoticed manufacture defects and extreme weather conditions. For this reason, regular fault detection is highly desirable to ensure the return on investment (ROI) of both small and utility scale PV installations. However, frequency and the level of detail of an inspection is often limited by available work force and cost. Electroluminescence (EL) imaging can be used to rapidly and accurately detect a large range of major and minor faults in PV modules such as cell cracks, broken interconnections, PID among others [2], [3]. In other words, EL imaging can reveal many faults often not detectable by current field inspection methods such as infrared thermography or electrical characterization. State-of-the-art EL image acquisition however faces crucial technical limitations, including long exposure times and low signal-to-noise ratio (SNR) under sun irradiation.

The most commonly used cameras for EL imaging have silicon-based detectors (such as a CCD), which present a weak spectral sensitivity in the EL emission range of crystalline silicon solar cells. Although a high resolution can easily be achieved with these detectors, their long image exposure times (on the order of seconds) limit inspection time and their application in non-stationary systems such as in UAV. In contrast, cameras with InGaAs-based detectors have a good spectral response to the silicon luminescence emission and therefore shorter integration times, which can be even shorter 1 ms [4].

Background (BG) images are often necessary to correct for ambient light noise, and are strictly necessary when performing daylight EL. The capability to acquire many images per scene, with high frame rates, allows outdoor daylight EL acquisition to be performed in very short intervals or even in motion with proper image processing, such as motion estimation and compensation.

Research efforts are ongoing to develop a fully automated solar plant inspection method including UAV based EL imaging [2], [4]–[6]. To support this effort, the objective of this paper is to perform the image processing required to obtain a final EL image from an original EL video acquisition in motion, in a system that includes lock-in EL for daylight measurements. Such technical development requires fast image acquisition and extensive image processing, i.e. module recognition and segmentation allowing for motion compensation, for posterior averaging and background removal to enhance the SNR of the final EL images.

II. EXPERIMENTAL DETAILS AND METHODOLOGY

A. Test string and electrical contact

For this experiment, one PV module was mounted in a test string, which was highly damaged by potential-induced degradation (PID) and cell cracks. The module consisted of 72 mono-crystalline 12.7 cm cells, arranged in a 6 x 12 matrix. Although the experiment was performed in a test string, only one module is analysed in this work concerning motion compensation and image processing. The experiment was performed outdoors, under natural light during a mostly

cloudy day when the diffuse light contribution was roughly 80% of the total global irradiance. The modules were installed facing south at 60 degrees inclination.

The outdoor EL setup, which consisted of a DC power supply unit (PSU), a PV module connected to a modulating (lock-in) box (Fig. 1). Such system synchronizes the image acquisition with an electrical forward bias applied by the DC power supply. The camera triggering was synchronized remotely via a 2.4 GHz Arduino Nano radio frequency module located in the EL lock-in modulation box. This wireless communication was designed for UAV applications, where the camera will be controlled by an embedded PC and powered by the UAV battery. The modulation frequency is programmable and driven by an Arduino logic controller. The pulse width modulated (PWM) waveforms applied to the PV panels in two different scenarios concerning the control of the camera can be seen in Fig. 2. Scenario 1 corresponds to the camera trigger in synchronization with the PV device under test (DUT) bias signal, while Scenario 2 corresponds to an unsynchronized signal, so the camera was able to acquire as many images as possible (in practice 4-5 per EL/BG state of the of the DUT bias) during the motion.
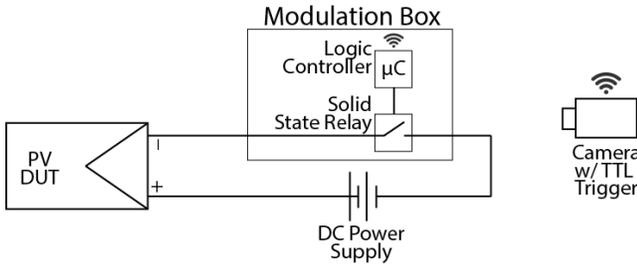

Fig. 1. Panels and modulation box connection circuit. The camera synchronization was performed via radio communication with the logic controller.
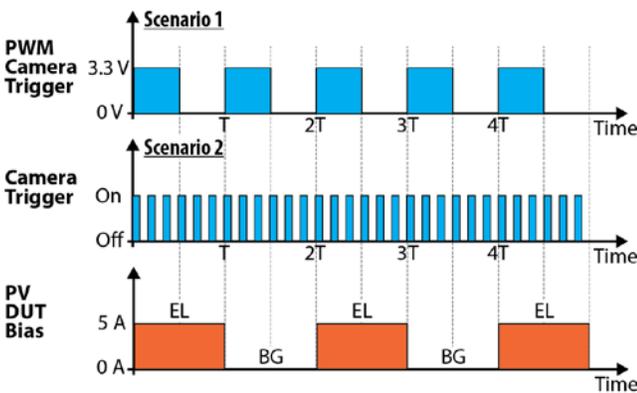

Fig. 2. PWM waveforms driven by the logic controller. The rising edges in the camera trigger waveforms correspond to when the image acquisition begins. Scenario 2 has the camera controlled by the internal trigger (see text for details).

B. Camera and motion setup

An InGaAs camera with 640 x 512 resolution and 14 bits dynamic range from Raptor Photonics model Owl640 is used for the experiment. A PC connected to the camera was required for image data acquisition and settings control. The EL images were acquired at 25 Hz PWM trigger frequency, which corresponds to a PSU frequency of 12.5 Hz. The exposure time was fixed for both scenarios (1 ms) and frame rate were 25 fps in Scenario 1 (controlled by the PWM camera trigger) and 120 fps in Scenario 2 (settled at the camera software – see Fig. 2). Note that the rising edges in the camera trigger waveforms correspond to when the image acquisition begins.

The luminescence emission peak for silicon-based solar cells at ambient temperature is centred at 1150 nm [7], therefore, to avoid detecting light from the sun and surroundings, an OD>4.0 1150nm band-pass filter with 50nm FWHM was used. A 25 mm fixed focus sapphire lens, without aperture control, was used, and in order to photograph the whole panels in vertical position, the camera was placed at approximately five meters from the test string, so a full module in portrait position could fit in the field of view.

The camera was fixed to a dolly equipped with wheels and placed on rails (Fig. 3). This mount allowed the acquisition of EL images at fixed distance from the PV modules, while the camera was moved in parallel along the length of the string. The camera was moved manually during images sequence acquisition at a speed of approximately 1 m/s, controlled with a stopwatch.
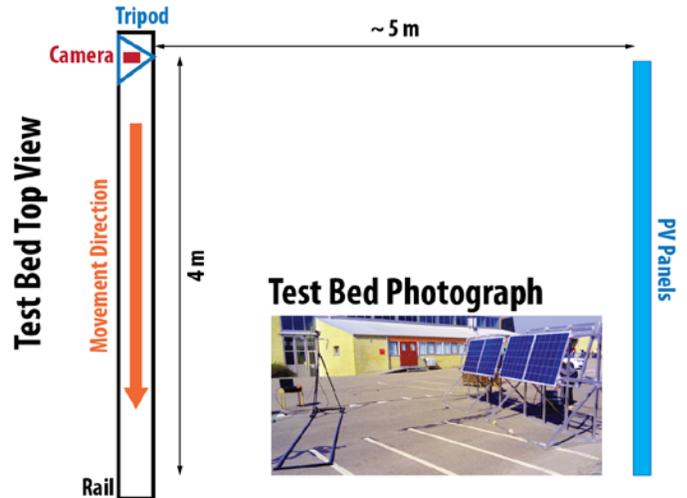

Fig. 3. Outdoor EL movable test bed. Top view diagram and photograph in the inset.

C. Image processing for motion compensation

To increase the quality of images for better failure diagnostic, EL and BG images are often averaged separately and the resulting EL_{AVG} and BG_{AVG} and then subtracted. A

priori to those averaging and subtracting operations, due to the non-stationary acquisition, numerous image-processing steps are required, and the automation of this process is ongoing. The programing steps to process the EL and BG images developed for this work include:

    i.   Identification of images containing the complete module
   ii.   Module edges and corner recognition;
  iii.   Module segmentation and cropping to region of interest;
  iv.   Split of EL and BG images;
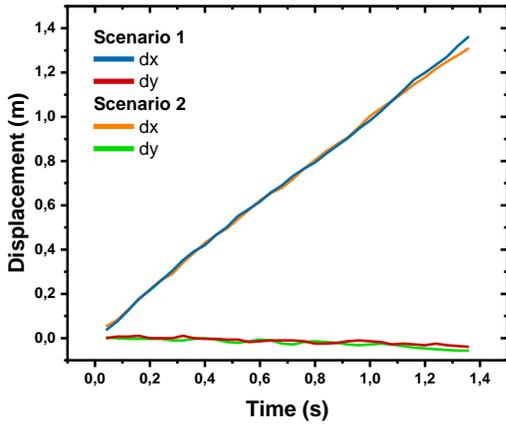   v.   Motion estimation and compensation;
  vi.   Averaging for denoising;
 vii.   EL and BG subtraction
viii.   Mapping to 8 bits and contrast correction for visualization.

From the image sequence (or video) acquired, the actual speed of the camera could be calculated from the computed motion shown in graph of Fig. 4. Even though the motion was manually induced, the speed is shown to be adequately constant throughout the image acquisition. Displacement on the y-axis along the image sequence was due to vibrations during the motion on the x-axis and it was also compensated for. On average, the images in motion analyzed in this work were captured at 0.97 m/s, here on referred as ~1 m/s for simplification.

Fig. 4. Computed motion compensation for the image sequence acquired with the test bed illustrated in Fig.3.

IV. RESULTS AND DISCUSSION

The EL images acquired in motion outdoors, after image processing are shown in Fig. 5, together with its stationary EL image taken indoors with a high-resolution DSLR camera. The Scenario 1 represents the situation when the BG image is taken sequentially right after the EL image, minimizing alterations in the final image quality that might occur with ambient light variations, i.e. sun irradiance variation, what has been shown to have influence in EL daylight image acquisition [8]. Scenario 2 in the other hand represent the fast image acquisition up to the camera image acquisition limit, therefore acquiring the highest amount of images possible at the given speed. The camera motion speed (~1 m/s) and the DUT lock-in frequency (25 Hz) was kept the same for both scenarios. In
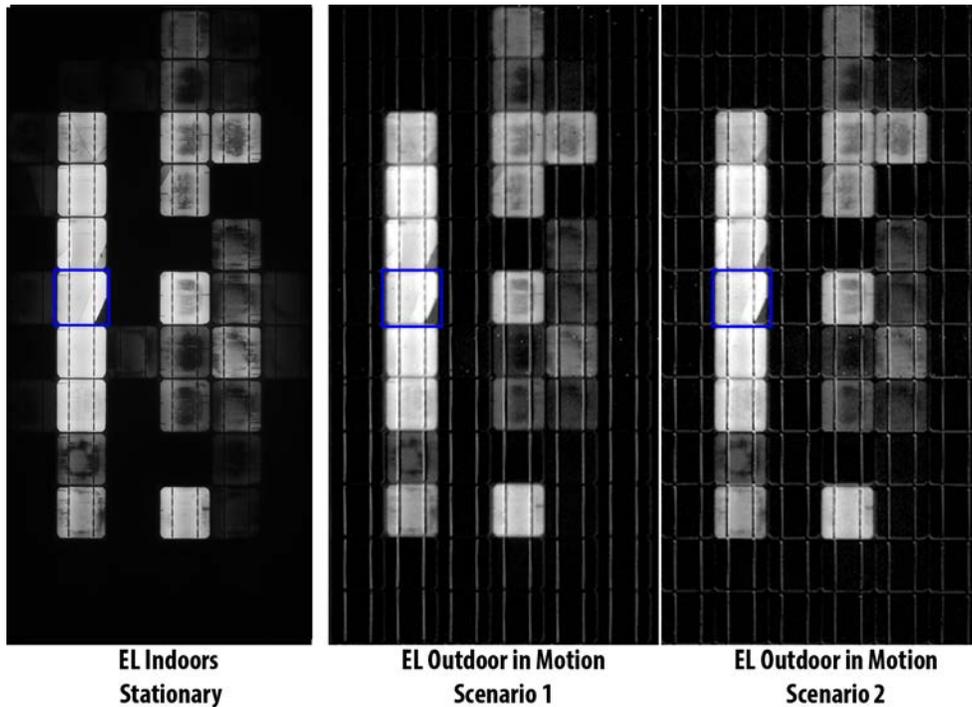

Fig. 5. EL image acquired indoors at stationary conditions compared with outdoor EL images acquired in motion (~1 m/s) using synchronized (Scenario 1) and unsynchronized (Scenario 2) lock-in and camera triggering after image processing (see text for further details).

the Scenario 1, the amount of images available for averaging were 34, i.e. 17 EL and 17 BG images. In the Scenario 2, the amount of images available were 162, or 81 EL and 81 BG images. While 34 images may be limiting for EL imaging at high sun irradiance, 162 images offers more than enough images for averaging and SNR enhancement to obtain EL images at >900 W/m^2 GHI and strong direct beam [8]. Even though the indoors EL is performed with a much higher resolution camera, the outdoors EL final images acquired in motion show very similar level of details. For the sun irradiance and weather conditions at the moment of the test (overcast), the higher amount of images available in Scenario 2 did not add on the obtained visual quality than the images available in Scenario 1, therefore not all available images from Scenario 2 were used to obtain the resulting image Fig. 5. The SNR$_{50}$ calculated for the resulting images (following the guidelines from [9] and the extension proposed on [10]) was 7.9 for Scenario 1 using 34 images and 6.7 for Scenario 2 using 44 images. These values tend to change considerably with the measurement conditions, combined with camera settings and bias, what suggests further investigation concerning specific factors in the future. We can discern the shunted cells typically in the edges of a module affected by PID, and cracks in several of the not completely shunted cells.

The resulting images still present a certain level of pixel mismatch after the motion compensation, easily verified by observing the ribbon and interconnection that would not appear after subtraction if the pixel displacement were accurate over the whole module. The motion compensation was more accurate on the top of the module than on the bottom (in the x-axis). Independent of the scenario characteristics itself, but possibly due to the higher amount of images used, the Scenario 2 EL image exhibited a mismatch also in the y-axis after the applied correction detected as shown in the graph of Fig. 4. Those mismatches are due to perspective distortion and can be compensated for after the module segmentation and motion compensation steps [11].

An important challenge for fast acquisition of outdoors EL is to detect minor failures using low resolution cameras, and for lock-in EL in motion, this play a decisive role to the obtainment of final EL image. We verified that the main information level provided by outdoors non-stationary EL is preserved even with minor displacements; however, it may compromise the detection of faults of little dimensions such as micro-cracks. In Fig. 6, the detail of the cracked cell 6B (coordinate defined following the guidelines at [9], indicated in Fig. 5 with a blue square) is shown for the same three EL images in Fig. 5. Cell 6B present a mode C crack in the bottom left corner, finger interruption in the top left and a mode A crack (or micro-crack) between the busbars. Even though some of the finger interruptions may be unclear in the outdoor EL images taken in motion, the micro-crack is observable as an apparent difference in shade when zoomed in for the automatic contrast correction applied.

In order to evaluate how the micro-crack appears in the final outdoor EL images taken in motion, in Fig. 7, the gray value profile from the corresponding red lines draw in Fig. 6 are presented. The EL Indoors stationary image had pixel resolution reduced to match the EL Outdoor camera resolution for comparison. Using the indoors stationary EL as guide (as the acquisition conditions, i.e. stationary, indoors, camera resolution and sharpness enhance considerable the image properties), we verify that the micro-crack is not well defined as a trough in the profile for the outdoor EL in motion as in the EL stationary. Instead, the gray value arises smoothly (from the right to the left), a better defined trough for Scenario 1, possibly due to its better pixel match. However, in the full module appearance, the micro-crack can be easily confirmed. This example shows that the final non-stationary EL image, due to its image quality, may be more challenging for automatic defect detection based on histogram analysis and/or gray value signature, and may require machine-learning tools for the task.

Finally, no blur effect from the individual non-stationary EL images were observed with acquisition made at 25 (Scenario 1) or 120 fps (Scenario 2) at the speed tested (~1 m/s).
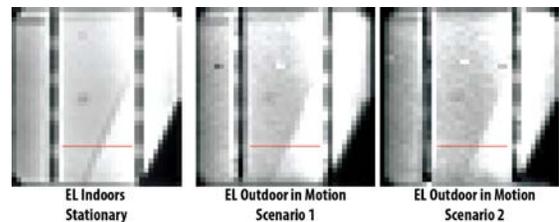

Fig. 6. Detail from cell 6B from the modules EL images shown in Fig. 5. EL Indoors stationary had pixel resolution reduced to match the EL Outdoor camera resolution for comparison.
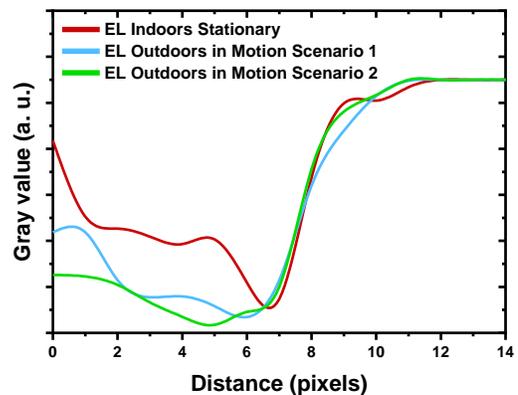

Fig. 7. Gray value profile over a micro-crack corresponding to the horizontal red line drawn in the EL images at Fig. 6.

V. CONCLUSION

In this work, we performed the experiment and the image processing steps to obtain outdoor lock-in EL images acquired in motion. The critical information regarding the state of the

active area of the PV modules was not only preserved in the processed non-stationary EL images, but very little dimension faults such as micro-cracks and finger interruptions were possible to be recognized. These results confirm the application of outdoor measurement of lock-in EL in motion suggested by Adams et al. [4] and is a step further towards fast EL acquisition in the field. The current speed recorded here would allow the lock-in EL image acquisition for 1 PV module per second, which corresponds to a minimum of 100 kW of PV modules inspected per hour, depending on the installation configuration.

While two different image acquisition scenarios have been performed here, the ideal scenario in daylight conditions will be the combination of both Scenarios 1 and 2, where ambient light interference can be avoided and the highest amount of images acquired. To allow efficient use of these resources, two image processing steps, i.e. module segmentation and perspective correction, should take place along with motion compensation.

The continuation of this work will further address the image processing and perform lock-in EL image acquisition with a movable test bed at different sun irradiance levels and faster speeds.

REFERENCES

[1] OCDE & IEA, "Market Report Series: Renewables 2017, analysis and forecats to 2022," J. Qual. Particip., vol. 104, no. 42, pp. 20142–20142, 2017.

[2] J. B. S. Koch, T. Weber, C. Sobottka, A. Fladung, P. Clemens, "Outdoor Electroluminescence Imaging of Crystalline Photovoltaic Modules: Comparative Study between Manual Ground-Level Inspections and Drone-Based Aerial Surveys," 32nd Eur. Photovolt. Sol. Energy Conf. Exhib., pp. 1736–1740, 2016.

[3] M. Köntges et al., "Review of Failures of Photovoltaic Modules," IEA-Photovoltaic Power Syst. Program., pp. 1–140, 2014.

[4] J. Adams et al., "Non-Stationary Outdoor EL-Measurements with a Fast and Highly Sensitive InGaAs Camera," 32nd Eur. Photovolt. Sol. Energy Conf. Exhib., 2016.

[5] C. Buerhop and H. Scheuerpflug, "Field inspection of PV-modules using aerial, drone-mounted thermography," 29th Eur. Photovolt. Sol. Energy Conf. Exhib., pp. 2975–2979, 2013.

[6] G. A. dos Reis Benatto et al., "Development of outdoor luminescence imaging for drone-based PV array inspection," IEEE Photovolt. Spec. Conf., 2017.

[7] T. Fuyuki, H. Kondo, T. Yamazaki, Y. Takahashi, and Y. Uraoka, "Photographic surveying of minority carrier diffusion length in polycrystalline silicon solar cells by electroluminescence," Appl. Phys. Lett., vol. 86, no. 26, pp. 1–3, 2005.

[8] G. A. dos Reis Benatto et al., "Luminescence imaging strategies for drone-based PV array inspection," 33rd Eur. Photovolt. Sol. Energy Conf. Exhib., pp. 2016–2020, 2017.

[9] IEC, "PNW/TS 82-901 Ed. 1.0 Photovoltaic devices - Part 13: Electroluminescence of photovoltaic modules (proposed future IEC TS 60904-13)." http://www.iec.ch/.

[10] C. Mantel et al., "SNR Study of Outdoor Electroluminescence Images under High Sun Irradiation," IEEE 7th World Conf. Photovolt. Energy Convers., pp. 2–4, 2018.

[11] C. Mantel et al., "Correcting for Perspective Distortion in Electroluminescence Images of Photovoltaic Panels," IEEE 7th World Conf. Photovolt. Energy Convers., 2018.